Inorg. Chem. **2002**, *41*, 796–804

Electronic Structures of Electron-Rich Octahedrally Condensed Transition-Metal Chalcogenide Clusters

Régis Gautier,[†,‡] Eric Furet,[†,‡] Jean-François Halet,[*,†] Zhenyang Lin,[*,§] Jean-Yves Saillard,[†] and Zhitao Xu[§]

Laboratoire de Chimie du Solide et Inorganique Moléculaire, UMR 6511 CNRS-Université de Rennes 1, Institut de Chimie de Rennes, 35042 Rennes Cedex, France, Département de Physicochimie, UPRES 1795, Ecole Nationale Supérieure de Chimie de Rennes, Institut de Chimie de Rennes, 35700 Rennes Cedex, France, and Department of Chemistry, Hong Kong University of Science and Technology, Clear Water Bay, Kowloon, Hong Kong, P. R. China

Received July 30, 2001

The electronic structures of some electron-rich octahedrally condensed transition-metal chalcogenide clusters are analyzed with the aid of extended Hückel and density functional molecular orbital calculations. A simple orbital approach is developed to analyze the electron counts of these clusters, which do not obey any existing electron-counting rules. Different electron counts are allowed, depending upon the nature of the metal. Optimal counts are discussed. Metal–metal bonding is generally weak in these species. Consequently, their structural arrangements are mainly governed by metal–ligand interactions.

Introduction

Polynuclear late-transition-metal chalcogenide cluster compounds have attracted considerable interest over the past few years from different fields because of their various properties. For instance, nickel−chalcogenide cluster complexes are important in biological processes because they play a role in the properties of the active centers of many enzymes.[1] In nanoscience, large ligand-stabilized transition-metal chalcogenide clusters can be regarded as nanoscaled cutouts of bulk transition-metal chalcogenides that may offer applications in nanoelectronics.[2] A large number of such species have been synthesized and structurally characterized.[3] Structures **1**−**5** represent some of these octahedrally based polynuclear cluster complexes (see Table 1 for a partial list).[3−19] Like the topologies of the "Chevrel phases" compounds,[20,21] topologies of these clusters more closely resemble cylinders than spheres. Clusters **1**−**5** are all electron-rich. Most of them have electron counts that are not satisfactorily explained within the existing electron-counting rules.[22] In other words, no complete pictures of their electronic structures have yet emerged.

In an effort to establish relationships between the observed geometry and the bonding of molecular, polynuclear, transition-metal chalcogenide cluster complexes, we have already provided bonding pictures based on the orbital interaction concept for some transition-metal chalcogenide clusters with different structural arrangements. The bonding in the unprecedented pentagonal sulfide cluster $[Ni_5(\mu_5\text{-}S)(\mu\text{-}SR)_5]^-$ [23] was analyzed.[24] The electronic structures of empty and

* Corresponding authors. E-mail: halet@univ-rennes1.fr; chzlin@usthk.hk.
† Université de Rennes 1.
‡ Ecole Nationale Supérieure de Chimie de Rennes.
§ Hong Kong University of Science and Technology.

(1) *The Bioinorganic Chemistry of Nickel*; Lancaster, J. R., Ed.; VCH: Weinheim, 1988.
(2) *Clusters and Colloids: From Theory to Applications*; Schmid, G., Ed.; VCH: Weinheim, 1994.
(3) See for example: (a) Fenske, D.; Ohmer, J.; Hachgenei, J.; Merzweiler, K. *Angew. Chem., Int. Ed. Engl.* **1988**, *27*, 1277. (b) Fenske, D. In *Clusters and Colloids: From Theory to Applications*; Schmid, G., Ed.; VCH: Weinheim, 1994; p 212. (c) Henkel, G.; Weissgraeber, S. In *Metal Clusters in Chemistry*; Braunstein, P., Oro, L. A., Raithby, P. R., Eds.; Wiley-VCH: Weinheim, 1999; Vol. 1, p 163.
(4) (a) Agresti, A.; Bacci, M.; Cecconi, F.; Ghilardi, C. A.; Midollini, S. *Inorg. Chem.* **1985**, *24*, 689. (b) Bencini, A.; Ghilardi, C. A.; Midollini, S.; Orlandini, A.; Russo, U.; Uytthoeven, M. G.; Zanchini, C. *J. Chem. Soc., Dalton Trans.* **1995**, 963.
(5) Cecconi, F.; Ghilardi, C. A.; Midollini, S.; Orlandini, A. *J. Chem. Soc., Dalton Trans.* **1987**, 831.
(6) Steigerwald, M. L.; Siegrist, T.; Gyorgy, E. M.; Hessen, B.; Kwon, Y.-U.; Tanzler, S. M. *Inorg. Chem.* **1994**, *33*, 3389.
(7) (a) Fenske, D.; Hachgenei, J.; Ohmer, J. *Angew. Chem., Int. Ed. Engl.* **1985**, *24*, 706. (b) Fenske, D.; Ohmer, J.; Merzweiler, K. *Z. Naturforsch., B.: Chem. Sci.* **1987**, *42*, 803.
(8) Cecconi, F.; Ghilardi, C. A.; Midollini, S.; Orlandini, A.; Zanello, P. *Polyhedron* **1986**, *5*, 2021.
(9) Cecconi, F.; Ghilardi, C. A.; Midollini, S.; Orlandini, A.; Zanello, P.; Cinquantini, A.; Bencini, A.; Uytterhoeven, M. G.; Giorgi, G. *J. Chem. Soc., Dalton Trans.* **1995**, 3881.

10.1021/ic010812b CCC: $22.00
Published on Web 01/29/2002

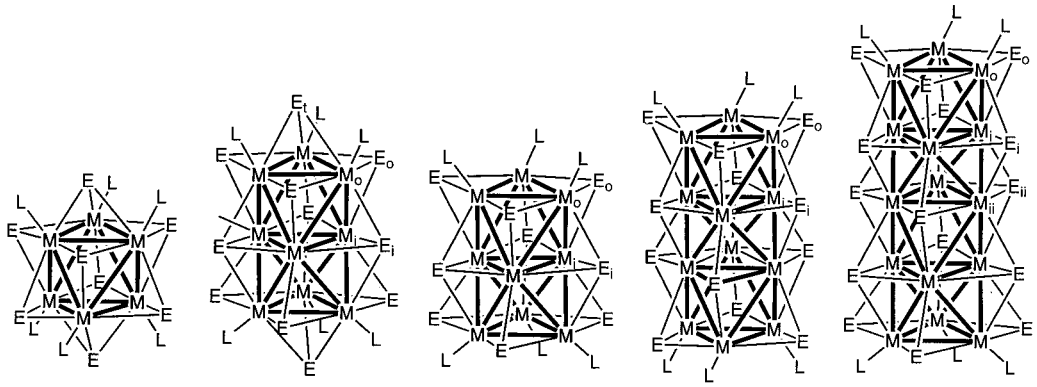

1 **2** **3** **4** **5**

metal-centered hexacapped cubic species such as $Ni_8(\mu_4\text{-}S)_6(PPh_3)_8$,[25] $Ni_8(\mu_9\text{-}Ni)(\mu_4\text{-}Te)_6(PEt_3)_8$,[26] and related species were well-studied.[27] The bonding picture of the very complicated high-nuclearity cluster $[Ni_{20}Se_{12}(SeMe)_{10}]^{2-}$ [28] was also discussed.[24] Continuing our efforts, we provide in this contribution a bonding analysis for the octahedrally based clusters **1**−**5**, with the aid of extended Hückel theory (EHT) and density functional theory (DFT) calculations (see the Appendix for computational details).

The approach here is to employ a simple and unified molecular orbital model based on metal−metal bonding that arises from the interaction of the frontier orbitals of individual metal fragments that are derived from local metal−ligand coordination. This kind of "local metal frontier orbital" approach has proven to be extremely successful in understanding the metal−metal interactions of transition-metal clusters containing mainly π-donating ligands.[29,30] The traditional approach is to first consider metal−metal orbital interactions of the metal core together with the interactions of the terminal ligands and then to introduce the bridging ligands' orbitals to obtain the overall orbital interaction diagram.[27,31−32] The advantage of the local metal frontier orbital approach is that it considers the local metal−ligand interaction first. Therefore, some metal d orbitals may be safely neglected in considering the M−M interactions because they are mainly involved in metal−ligand bonding. Thus, the metal−metal orbital interactions are significantly simplified because the total number of available fragment frontier orbitals is enormously reduced.[29,30] Hughbanks and Hoffmann, in their detailed bonding discussion of the Chevrel phases compounds that are based on the same structural principle as are species **1**−**5**,[21] elegantly explained that the involvement of some metal d orbitals that are used for metal−ligand bonding in M−M interactions may be neglected.

Face-Bridged Octahedral $M_6(\mu_3\text{-}E)_8L_6$ Species. The $M_6(\mu_3\text{-}E)_8L_6$ arrangement (**1**) is typical for face-bridged octahedrally based cluster species. Electron-rich $M_6(\mu_3\text{-}E)_8L_6$ species based on this structural arrangement have been characterized with M = Fe, Co, or Pd, E = S, Se, or Te, L = PR_3 or CO, and different metallic electron (ME) or cluster valence electron (CVE) counts[33] (see Table 1). Because octahedral $M_6(\mu_3\text{-}E)_8L_6$ clusters appear in both the molecular and solid states and have various physical properties, they have been extensively studied from a theoretical viewpoint.[15,29] The main results of those studies are briefly recalled here for those compounds containing late transition

(10) Diana, E.; Gervasio, G.; Rossetti, R.; Valdemarin, F.; Bor, G.; Stanghellini, P. L. *Inorg. Chem.* **1991**, *30*, 294.
(11) Jiang, F.; Huang, X.; Cao, R.; Hong, M.; Liu, H. *Acta Crystallogr., Sect. C* **1995**, *51*, 1275.
(12) Gervasio, G.; Kettle, S. F. A.; Musso, F.; Rossetti, R.; Stanghellini, P. L. *Inorg. Chem.* **1995**, *34*, 298.
(13) Fenske, D.; Ohmer, J.; Hachgenei, J. *Angew. Chem., Int. Ed. Engl.* **1985**, *24*, 993.
(14) Steigerwald, M. L.; Siegrist, T.; Stuczynski, S. M. *Inorg. Chem.* **1991**, *30*, 4940.
(15) Cecconi, F.; Ghilardi, C. A.; Midollini, S.; Orlandini, A.; Bencini, A. *J. Chem. Soc., Dalton Trans.* **1996**, 3991.
(16) Vogt, K. Ph.D. Thesis, University of Karlsruhe, Germany, 1994.
(17) Cecconi, F.; Ghilardi, C. A.; Midollini, S. *Inorg. Chem.* **1983**, *22*, 3802.
(18) Fenske, D.; Ohmer, J. *Angew. Chem., Int. Ed. Engl.* **1987**, *26*, 148.
(19) Hong, M.; Huang, Z.; Liu, H. *J. Chem. Soc., Chem. Commun.* **1990**, 1210.
(20) Chevrel, R.; Sergent, M.; Prigent, J. *Solid State Chem.* **1971**, *3*, 515.
(21) (a) Hughbanks, T.; Hoffmann, R. *J. Am. Chem. Soc.* **1983**, *105*, 1150. (b) Hughbanks, T. *Prog. Solid State Chem.* **1989**, *19*, 329.
(22) (a) Mingos, D. M. P.; Johnston, R. L. *Struct. Bonding (Berlin)* **1987**, *68*, 29. (b) Mingos, D. M. P.; Wales, D. J. *Introduction to Cluster Chemistry*; Prentice Hall: Englewood Cliffs, 1990.
(23) Müller, A.; Henkel, G. *J. Chem. Soc., Chem. Commun.* **1996**, 1005.
(24) Cheung, F.-W.; Lin, Z. *Angew. Chem., Int. Ed. Engl.* **1997**, *36*, 1847.
(25) Fenske, D.; Krautscheid, H.; Müller, M. *Angew. Chem., Int. Ed. Engl.* **1992**, *31*, 321.
(26) Brennan, J. G.; Siegrist, T.; Stuczynski, S. M.; Steigerwald, M. L. *J. Am. Chem. Soc.* **1989**, *111*, 9240.
(27) (a) Furet, E.; Le Beuze, A. L.; Halet, J.-F.; Saillard, J.-Y. *J. Am. Chem. Soc.* **1994**, *116*, 274. (b) Furet, E.; Le Beuze, A. L.; Halet, J.-F.; Saillard, J.-Y. *J. Am. Chem. Soc.* **1995**, *117*, 4936. (c) Halet, J.-F.; Saillard, J.-Y. *Struct. Bonding (Berlin)* **1997**, *87*, 81. (d) Zouchoune, B.; Ogliaro, F.; Halet, J.-F.; Saillard, J.-Y.; Eveland, J. R.; Whitmire, K. H. *Inorg. Chem.* **1998**, *37*, 865. (e) Gautier, R.; Halet, J.-F.; Saillard, J.-Y. *Eur. J. Inorg. Chem.* **1999**, 673. (f) Gautier, R.; Ogliaro, F.; Halet, J.-F.; Saillard, J.-Y.; Baerends, E. J. *Eur. J. Inorg. Chem.* **1999**, 1161. (g) Gautier, R.; Halet, J.-F.; Saillard, J.-Y. In *Metal Clusters in Chemistry*; Braunstein, P., Oro, L., Raithby, P. R., Eds.; Wiley-VCH: Weinheim, 1999; Vol. 3, p 1643. (h) Garland, M. T.; Halet, J.-F.; Saillard, J.-Y. *Inorg. Chem.* **2001**, *40*, 3342.
(28) Fenske, D.; Fischer, A. *Angew. Chem., Int. Ed. Engl.* **1995**, *34*, 307.
(29) (a) Lin, Z.; Williams, I. D. *Polyhedron* **1996**, *15*, 3277. (b) Bencini, A.; Fabrizi de Biani, F.; Uytthoeven, M. G. *Inorg. Chim. Acta* **1996**, *244*, 231. (b) Lin, Z.; Fan, M.-F. *Struct. Bonding (Berlin)* **1997**, *87*, 35, and references therein. (c) Arratia-Perez, R.; Hernandez-Acevedo, L. *J. Chem. Phys.* **1999**, *111*, 168.
(30) Xu, Z.; Lin, Z. *Chem.−Eur. J.* **1998**, *4*, 28.
(31) Jiang, Y.; Tang, A.; Hoffmann, R.; Huang, J.; Lu, J. *Organometallics* **1985**, *4*, 27.
(32) Johnston, R. L.; Mingos, D. M. P. *Inorg. Chem.* **1986**, *25*, 1661.

Table 1. Examples of Electron-Rich Octahedrally Based Metal Chalcogenide Clusters

cluster	ME (CVE)[a]	M oxidn state[b]	d_{M-M} (Å)[c]	ref
$[Fe_6(\mu_3\text{-}S)_8(PEt_3)_6]^{2+}$ (**1**)[d]	30 (90)	+3.0	2.617/2.610	4
$[Fe_6(\mu_3\text{-}S)_8(PEt_3)_6]^{+}$ (**1**)	31 (91)	+2.83	2.636	5
$Fe_6(\mu_3\text{-}Te)_8(PMe_3)_6$ (**1**)	32 (92)	+2.67	2.818/2.972	6
$[Co_6(\mu_3\text{-}S)_8(PPh_3)_6]^{+}$ (**1**)	37 (97)	+2.83	2.819/2.901	7
$[Co_6(\mu_3\text{-}S)_8(PEt_3)_6]^{+}$ (**1**)	37 (97)	+2.83	2.794/2.739	8, 9
$Co_6(\mu_3\text{-}S)_8(CO)_6$ (**1**)	38 (98)	+2.67	2.811	10
$Co_6(\mu_3\text{-}S)_8(PPh_3)_6$ (**1**)	38 (98)	+2.67	2.87	11
$Co_6(\mu_3\text{-}S)_8(PEt_3)_6$ (**1**)	38 (98)	+2.67	2.816	8
$Co_6(\mu_3\text{-}S)_8(PnBu_3)_6$ (**1**)	38 (98)	+2.67	2.815	3
$Co_6(\mu_3\text{-}Se)_8(CO)_6$ (**1**)	38 (98)	+2.67		12
$Co_6(\mu_3\text{-}Se)_8(PPh_3)_6$ (**1**)	38 (98)	+2.67	3.009	13
$Co_6(\mu_3\text{-}Se)_8(PnBu_3)_6$ (**1**)	38 (98)	+2.67	2.946	3
$Co_6(\mu_3\text{-}Te)_8(PEt_3)_6$ (**1**)	38 (98)	+2.67	3.22	14
$[Co_6(\mu_3\text{-}Te)_8(PEt_3)_6]^{2+}$ (**1**)	36 (96)	+3.00	3.005−3.265	15
$[Pd_6(\mu_3\text{-}S)_8(PPh_3)_6]^{4-}$ (**1**)	48 (108)	+2.0	2.89−3.02	16
$Co_9(\mu_4\text{-}Se)_3(\mu_3\text{-}Se)_8(PPh_3)_6$ (**2**)	59 (137)	+2.44	2.71−2.97	13
$[Ni_9(\mu_4\text{-}S)_3(\mu_3\text{-}S)_6(PEt_3)_6]^{2+}$ (**3**)	70 (136)	+2.22	2.681−2.960	17
$Ni_{12}(\mu_4\text{-}Se)_6(\mu_3\text{-}Se)_6(PEt_3)_6$ (**4**)	96 (180)	+2.0	2.72−2.97	18
$Ni_{15}(\mu_4\text{-}Se)_9(\mu_3\text{-}Se)_6(PPh_3)_6$ (**5**)	120 (222)	+2.0	2.70−3.02	18
$Ni_{15}(\mu_4\text{-}S)_9(\mu_3\text{-}S)_6(PPh_3)_6$ (**5**)	120 (222)	+2.0	2.644−2.918	19

[a] Metallic electron and cluster valence electron counts (see ref 33). [b] Averaged oxidation state of M. [c] Averaged. [d] Structural arrangement (see structures **1**−**5**).

metals.[4,9,34−35] In such compounds, each transition-metal center is locally bound to five ligands, which depicts a square-pyramidal arrangement. For a square-pyramidal ML_5 fragment, the frontier orbitals (FO) consist of a σ-type hybrid orbital (hy(σ)) and a set of three orbitals that are mainly d in character, two of which have π symmetry and one of which has δ symmetry (t_{2g}), as shown on the left-hand side of Figure 1.[36]

Figure 1 shows also the qualitative molecular orbital interaction diagram for the 38-ME model $Co_6(\mu_3\text{-}Se)_8(PH_3)_6$ (**1-Co**) of O_h pseudosymmetry obtained from EHT calculations. (The real symmetry group is D_{3d} because of the local symmetry of the PH_3 groups.) The orbital interactions among the six hy(σ) frontier orbitals of the ML_5 fragments give rise to one strongly bonding (a_{1g}), three nonbonding (t_{1u}), and two antibonding (e_g) combinations. The d(π) FOs of the six units generate sets of six in-phase (t_{2g} and t_{1u}) and six out-of-phase combinations (t_{1g} and t_{2u}). Finally, the six d(δ) FOs give rise to two bonding (e_g) and three nonbonding (t_{2u}) combinations and one antibonding (a_{2g}) combination. Second-order mixing between combinations of the same symmetry results in additional stabilization of the bonding π-type t_{1u}

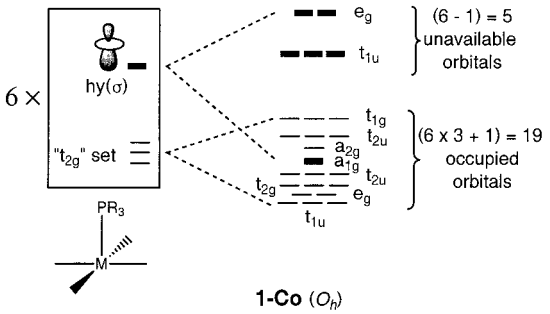

Figure 1. Qualitative molecular orbital interaction diagram for $Co_6(\mu_3\text{-}Se)_8(PH_3)_6$ (**1-Co**). For clarity in this and in Figures 3, 4, 6, and 7, thicker bars represent orbitals derived from the σ-type frontier hybrid orbitals and thinner bars represent orbitals derived from the d-type metallic FOs.

and δ-type e_g levels, whereas the nonbonding σ-type t_{1u} and antibonding σ-type e_g combinations are destabilized and become more antibonding.

The molecular orbitals derived from the t_{2g} sets in metal carbonyl clusters are usually taken as nonbonding because of the strong stabilization by the carbonyls' vacant π orbitals. In many face-bridged clusters, however, the t_{2g} frontier orbitals are very important in metal−metal bonding because of the bridging ligands that are π donors.[32] This situation is particularly common in the early-transition-metal clusters;[29,30] consequently, one might expect that for the electron-rich clusters given in Table 1 that also contain π-donor ligands, the t_{2g} frontier orbitals are also important. However, this is not the case. The t_{2g} frontier orbitals of late transition-metal atoms such as Fe and Co are contracted and thus give rise to a narrow band of MOs that, if filled, are rather inactive in metal−metal bonding, like those in metal carbonyl clusters. Therefore, the "metallic" orbital pattern of the 38-ME cluster model **1-Co** consists of a set of 18 occupied and overall nonbonding orbitals (a_{2g}, e_g, t_{1g}, t_{2g}, t_{1u}, and 2 t_{2u} (2 a_{2g}, 3 e_g, a_{1g}, a_{2u}, 2 a_{1u}, and 3 e_u in D_{3d} symmetry)) plus an occupied orbital (a_{1g} in D_{3d} symmetry)) with strong metal−metal bonding character separated from a vacant, antibonding, high-lying set of 5 MOs (e_g and t_{1u} (e_g, a_{2u}, and e_u in D_{3d} symmetry)). As noted earlier, the antibonding character of the latter is enhanced by some second-order mixing with low-lying MOs of the same symmetry.

This analysis is supported by DFT calculations carried out on **1-Co**. Full geometry optimization was made under the D_{3d} symmetry constraint. The optimized bond lengths for this model are given in Table 2. Remarkably, the computed distances are in rather good agreement with those measured experimentally in the 38-ME species $Co_6(\mu_3\text{-}Se)_8(PR_3)_6$ (R = Ph, *n*-Bu) (see Table 2).[4,13] The largest deviation concerns the Co−Se distances, which were computed to be ca. 0.07 Å longer than the experimental values. The DFT-MO diagram of the optimized geometry of **1-Co** is illustrated on the left-hand side of Figure 2. A closed-shell electron configuration analogous to that obtained with EHT calculations was computed for the 38 MEs with a HOMO−LUMO gap of 1.05 eV.

From this analysis, it can be concluded that the 38-ME $Co_6(\mu_3\text{-}E_8)L_6$ clusters have only one occupied strong metal−metal bonding MO, which is responsible for most of the 12

(33) There are different ways to count electrons in transition-metal clusters. One way is to consider the total cluster valence electron (CVE) count, which is obtained by adding the number of valence electrons for each metal atom and the electrons brought by the ligands involved in the metal−ligand bonds, augmented from one electron per negative charge or diminished from one electron per positive charge. An alternative way is to consider the metal electron (ME) count. These electrons are located in MOs that are mainly metallic in character. Among these electrons are those that are responsible for metal−metal bonding. Assuming an ionic bonding mode between oxidized metal atoms and anionic surrounding ligands, this ME count is obtained by adding the remaining number of valence electrons of the oxidized metal atoms in their actual oxidation states.

(34) Bencini, A.; Ghilardi, C. A.; Orlandini, A.; Midollini, S.; Zanchini, C. *J. Am. Chem. Soc.* **1992**, *114*, 9898.
(35) Mealli, C.; Lopez, J. A.; Sun, Y.; Calhorda, M. J. *Inorg. Chim. Acta* **1993**, *213*, 199.
(36) Elian, M.; Hoffmann, R. *Inorg. Chem.* **1975**, *14*, 1058.

Table 2. Comparison between Some Averaged Experimental Distances of $Co_6Se_8(PPh_3)_6$ and $Co_9Se_{11}(PPh_3)_6$ and the Computed Distances for $Co_6Se_8(PH_3)_6$(**1-Co**), $Co_9Se_{11}(PH_3)_6$ (**2-Co**), and $[Co_9Se_{11}(PH_3)_6]^+$ (**2-Co**$^+$)

distance	$Co_6Se_8(PPh_3)_6$, (Å)	$Co_6Se_8(PH_3)_6$ (**1-Co**), (Å)	$Co_9Se_{11}(PPh_3)_6$, (Å)	$Co_9Se_{11}(PH_3)_6$ (**2-Co**), (Å)	$[Co_9Se_{11}(PH_3)_6]^+$ (**2-Co**$^+$), (Å)
			intratriangle		
Co_o-Co_o[a]	3.01	3.01	2.92	2.85	2.85
Co_i-Co_i			2.82	3.04	3.05
			intertriangle		
Co_o-Co_i	3.00	2.91	2.79	2.83	2.82
			intratriangle		
Co_o-Se_o	2.35	2.44	2.35	2.43	2.43
Co_i-Se_i		2.42	2.35	2.42	2.43
Co_o-Se_t	2.35	2.42	2.34	2.38	2.34
Co−P	2.17	2.14	2.19	2.18	2.19

[a] See structure **2** for the labels on the atoms.

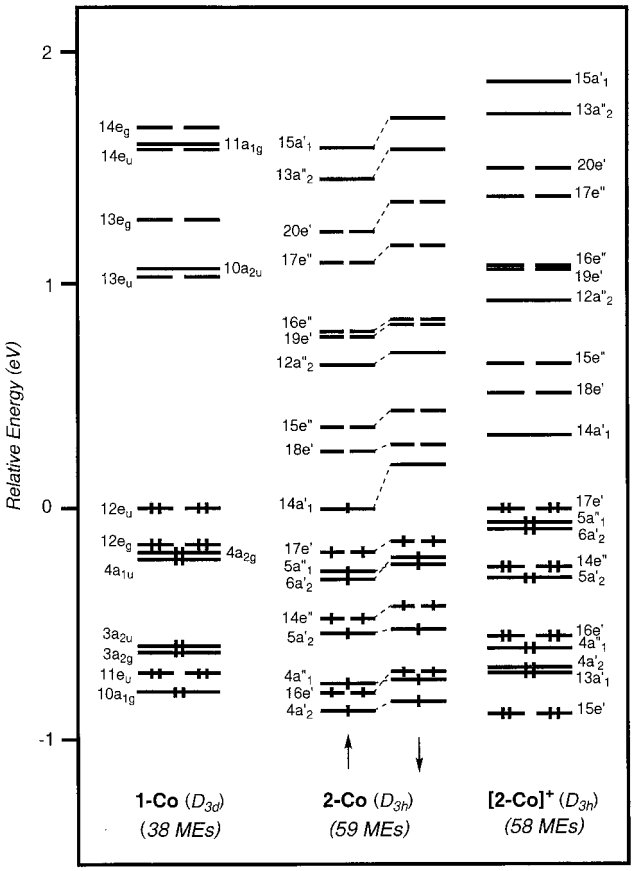

Figure 2. DFT-MO diagrams for $Co_6(\mu_3\text{-}Se)_8(PH_3)_6$ (**1-Co**) (left), $Co_9(\mu_4\text{-}Se)_3(\mu_3\text{-}Se)_8(PH_3)_6$ (**2-Co**) (middle), and $[Co_9(\mu_4\text{-}Se)_3(\mu_3\text{-}Se)_8(PH_3)_6]^+$ (**2-Co**$^+$) (right).

Co−Co bonding contacts.[35] Consequently, metal−metal bonding is weak in such species, and metal−metal separations are quite long (ca. 15−20% longer than that in elementary metals) and sensitive to the surrounding ligands. For a given electron count, M−M distances vary quite significantly (up to 15%) with the size of the capping ligands (see Table 1). These chalcogenide ligands play the most important role in the stability of these clusters. Similar conclusions have been drawn from many experimental and theoretical studies.[3−16,34−35]

On the basis of the significant HOMO−LUMO gap computed for **1-Co** (see Figure 2), one would expect the late-transition-metal chalcogenide $M_6(\mu_3\text{-}E_8)L_6$ clusters to have an unambiguous electron count. However, this is not the case for several octahedral clusters in which the nonbonding HOMOs are not completely filled. Only weak Jahn−Teller instability is expected for these compounds because of the high atomic connectivity of the cluster cage, as also noted earlier for transition-metal cubic clusters.[27] Thus, we assume that the capping ligands are the decisive forces for such an octahedral architecture. This situation is illustrated in the Co−Co bond lengths in the 37-ME $[Co_6(\mu_3\text{-}S_8)(PR_3)_6]^+$ cations that are similar to those in the 38-ME $Co_6(\mu_3\text{-}S_8)(PR_3)_6$ species (see Table 1). The iron species with ME = 30−32 provide other examples of the partial occupation of the HOMOs that can lead to magnetic properties. For instance, it has been shown that the 31-ME $[Fe_6(\mu_3\text{-}S_8)(PEt_3)_6]^+$ compound is paramagnetic, with an $S = {}^7/_2$ spin state (that is, the compound has seven unpaired electrons).[4]

In summary, octahedral $M_6(\mu_3\text{-}E_8)L_6$ species can be characterized by a range of electron counts rather than by only one electron count. If the early-transition-metal clusters are also taken into account, ME counts from 20 to 48 in compounds such as $W_6(\mu_3\text{-}S_8)(PEt_3)_6$[37] (80 CVEs) and $[Pd_6(\mu_3\text{-}S)_8(PPh_3)_6]^{4-}$[16] (108 CVEs), respectively, have also been reported. M−M bonding will be maximized in these species with 24 MEs (84 CVEs). For example, M−M bonding in $[Mo_6(\mu_3\text{-}Cl_8)Br_6]^{2-}$[38] corresponds to the occupation of the bonding and nonbonding MOs of the t_{2g} band and to the bonding a_{1g} MO.[29] The count of 48 MEs corresponds to the full occupation of the metallic MOs, that is, the t_{2g} band, the a_{1g} MO, and the high-lying antibonding e_g and t_{1u} MOs (see Figure 1). Examination of Walsh diagrams indicates that closed-shell electron configurations with large HOMO−LUMO gaps exist for 24, 38, and 48 ME species (i.e., 84, 98, and 108 CVEs).

Condensed Octahedral $Co_9(\mu_4\text{-}Se)_3(\mu_3\text{-}Se)_8(PPh_3)_6$ Cluster. The characterization of $Co_9(\mu_4\text{-}Se)_3(\mu_3\text{-}Se)_8(PPh_3)_6$ some years ago[13] made it clear that the condensation of octahedra via common faces, which is largely exemplified in the ternary molybdenum chalcogenide solid-state materials A_xMo_{3n+3}-

(37) Saito, T.; Yoshikawa, A.; Yamagata, T.; Imoto, H.; Onoura, K. *Inorg. Chem.* **1989**, *28*, 3588.
(38) Healy, P. C.; Kepert, D. L.; Taylor, D.; White, A. H. *J. Chem. Soc., Dalton Trans.* **1973**, 646.

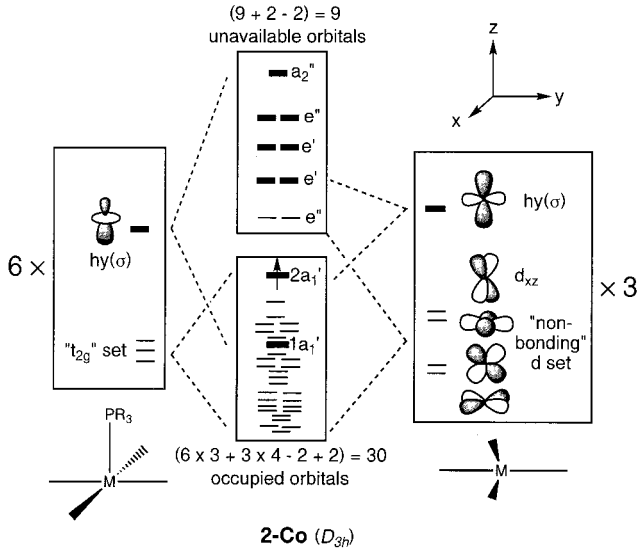

Figure 3. Molecular orbital interaction diagram for $Co_9(\mu_4\text{-}Se)_3(\mu_3\text{-}Se)_8(PH_3)_6$ (**2-Co**).

E_{3n+5},[39] could be extended to the more electron-rich transition metals. As its Mo_9E_{11} homolog indicates, this cluster consists of a staggered column of three metal triangles capped at each end. The cluster is composed of six square-pyramidal ML_5 fragments and three ML_4 fragments derived from a trigonal-bipyramidal complex by deleting one of the equatorial ligands.[36] The six square-pyramidal coordinated metal centers (outer, Co_o) form the upper and lower parts of the column, while the three remaining metal centers (inner, Co_i) form the middle triangle.

EHT calculations were first carried out on the 59-ME (137-CVE) cluster model $Co_9(\mu_4\text{-}Se)_3(\mu_3\text{-}Se)_8(PH_3)_6$ (**2-Co**) of D_{3h} symmetry. For each metal center in the three ML_4 fragments, the five FOs that are mainly d in character split into two nonbonding, two weakly antibonding (approximately nonbonding), and one antibonding hybrid orbitals.[36] The relevant splitting is shown on the right-hand side of Figure 3, where the thicker bar denotes hy(σ). Of the two weakly antibonding metal orbitals, d_{xz} lies higher in energy because the two ligands along the *z* axis bend away from the *yz* plane and thus increase its energy (see Figure 3 for the orientation of the Cartesian coordinate system, where the *z* axis is perpendicular to the plane containing the three metal centers of the ML_4 fragments).

The orbital interactions among the frontier orbitals of the nine fragments are schematically illustrated in Figure 3. The orbital interactions among the hy(σ) of the ML_5 and ML_4 fragments (thicker bars in Figure 3) show only one strongly bonding molecular orbital of a_1' symmetry ($1a_1'$), a situation that is also observed in other columnar clusters.[40] The other eight resulting MOs are antibonding overall after second-order mixing with low-lying d orbitals of the same symmetry, except one MO of a_1' symmetry ($2a_1'$) that is nearly nonbonding. Similar to the situation in **1-Co**, the orbital interactions among the t_{2g} sets of the ML_5 units and the nonbonding (and approximately nonbonding) FOs of the ML_4 units give rise to a metallic set of 30 levels. It is noteworthy that the highest energy level of e″ symmetry in this band is somewhat destabilized with respect to the others (an EHT energy gap of 0.87 eV was computed between this level and the level below ($2a_1'$)) and is rather close in energy to the antibonding levels descending from the hy(σ) FOs of the ML_5 and ML_4 fragments. A close examination of these e″ MOs indicates that they are metal−metal antibonding orbitals. One of their components is represented by **6**.

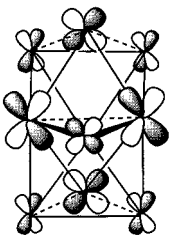

6

These MOs are predominantly derived from the high-energy fragment orbital d_{xz} of the ML_4 units that have weak metal−ligand antibonding character. The antibonding character between all neighboring metal atoms leads to significantly high energies.

DFT calculations were carried out on the **2-Co** model complex using different ME counts (58, 59, and 60) to support these conclusions. The results of geometry optimization on these models performed under D_{3h} symmetry are shown in Table 2, where pertinent structural parameters are listed and compared to those from the X-ray crystal structure of $Co_9Se_{11}(PPh_3)_6$.[13] The calculated bond distances in 2-Co are in rather good agreement with the averaged experimental values, except for the Co_i-Co_i distances that were computed to be 0.22 Å longer than the corresponding experimental distances. Surprisingly, the computed Co_i-Co_i distances are longer than the Co_o-Co_o distances, but the reverse is observed in the crystal structure.[13] We found no explanation for these results, except for the fact that the computed potential energy surface is rather flat near the energy minimum position, which indicates some flexibility for such an architecture, owing to rather weak M−M bonding. Removal of the unpaired electron in **2-Co**, which gives **2-Co**$^+$, does not induce severe alterations in the cluster geometry. Computed bond distances for the 59-ME **2-Co** and 58-ME **2-Co**$^+$ models are nearly identical. The Co_i-Co_i distances are slightly longer in **2-Co** than in **2-Co**$^+$ (see

(39) (a) Gougeon, P.; Potel, M.; Padiou, J.; Sergent, M. *Mater. Res. Bull.* **1987**, *22*, 1087. (b) Gougeon, P.; Potel, M.; Padiou, J.; Sergent, M. *Mater. Res. Bull.* **1988**, *23*, 453. (c) Gougeon, P.; Potel, M.; Sergent, M. *Acta Crystallogr., Sect. C* **1989**, *45*, 182. (d) Gougeon, P.; Potel, M.; Sergent, M. *Acta Crystallogr., Sect. C* **1989**, *45*, 1413. (e) Gougeon, P.; Potel, M.; Sergent, M. *Acta Crystallogr., Sect. C* **1990**, *46*, 2284. (f) Gougeon, P.; Picard, S.; Potel, M. *Acta Crystallogr., Sect. C* **1997**. (g) Thomas, C.; Picard, S.; Gautier, R.; Gougeon, P.; Potel, M. *J. Alloys Compd.* **1997**, *262*−*263*, 305. (h) Gautier, R.; Picard, S.; Gougeon, P.; Potel, M. *Mater. Res. Bull.* **1999**, *1*, 93. (i) Picard, S.; Gougeon, P.; Potel, M. *Angew. Chem., Int. Ed.* **1999**, *38*, 2034. (j) Picard, S.; Halet, J.-F.; Gougeon, P.; Potel, M. *Inorg. Chem.* **1999**, *38*, 4422. (k) Picard, S.; Saillard, J.-Y.; Gougeon, P.; Noel, H.; Potel, M. *J. Solid State Chem.* **2000**, *155*, 417. (l) Picard, S.; Gougeon, P.; Potel, M. *Acta Crystallogr., Sect. C* **2001**, *57*, 335.

(40) Lin, Z.; Mingos, D. M. P. *J. Organomet. Chem.* **1988**, *399*, 367.

Table 2). The ionization potentiel of the 59-ME species **2-Co** was computed to be 5.23 eV. Similarly, addition of one electron to **2-Co**, which gives the 60-ME **2-Co**$^-$ species, leads to Co−Co and Co−Se distances that are nearly identical to those found in **2-Co**. We note a slight lengthening of the Co−Co distances in the central metal triangle. The electron affinity of the 59-ME species **2-Co** was computed to be 2.30 eV.

The DFT-MO energy diagrams for **2-Co** (spin-unrestricted) and **2-Co**$^+$ are given on the middle and the right-hand side of Figure 2, respectively. The ground-state electron configuration $[136](a'_1)^1$ was computed for **2-Co**. The presence of this doublet ground state should be verified with further experiments. Less than 0.20 eV separates the occupied $14a'_1$ α-spin orbital from the vacant 18e′ α-spin orbitals. In other words, there is no clear energy separation between the set of metallic MOs and the antibonding set of MOs derived from the hy(σ) FOs of the constituent fragments. Here again, the high connectivity of the metal atoms and the bridging-ligand framework must prevent strong Jahn−Teller distortions from occurring. Depopulation of the $14a'_1$ MO leads to some modification of the electronic structure, as shown on the right-hand side of Figure 2. A small but substantial gap of 0.30 eV was computed for the 58-ME model **2-Co**$^+$ between the HOMO 17e′ and the LUMO $14a'_1$. The results of this calculation supports the possible existence of the cationic species $[Co_9Se_{11}(PPh_3)_6]^+$.

As noted earlier for the $M_6(\mu_3\text{-}E)_8L_6$ species (**1**), other electron counts for **2** must be possible because of the particular nature of the metallic orbital set, which is nonbonding overall when fully occupied. This situation is illustrated for the case of the recently reported condensed cluster $[Re_9(\mu_4\text{-}Se)_3(\mu_3\text{-}Se)_8Br_6]^{2-}$, which is characterized by 37 MEs (115 CVEs).[41] Counts of 32, 35.3, and 35.4 MEs are encountered in the solid-state materials *h*-Mo_9Se_{11}, $Ag_{2.3}$-$CsMo_9Se_{11}$, and $Ag_{4.4}ClMo_9Se_{11}$, respectively.[42] It is noteworthy that most of the condensed M_9 species possess an odd number of electrons. Maximum M−M bonding should occur when the strongly bonding cluster MO of a'_1 symmetry and roughly half of the metallic t_{2g} bands are occupied. Previous calculations on molybdenum chalcogenide clusters have indicated that maximum M−M bonding is attained for 36 MEs.[21,43] Consequently, with electron counts in the range of 32−37 MEs, M−M bond distances in the Mo and Re species are rather short, being comparable to M−M distances in elemental metals. On the other hand, with the metallic d band in $Co_9Se_{11}(PPh_3)_6$ almost filled, the Co−Co bond distances are appreciably longer than are those in metallic cobalt.

We wonder if counts larger than 59 MEs are possible for such an $M_9E_{11}L_6$ structural arrangement. These counts are possible, in principle, if we bear in mind that the 48-ME octahedral species $[Pd_6(\mu_3\text{-}S)_8(PPh_3)_6]^{4-}$[16] has a t_{2g} band, an

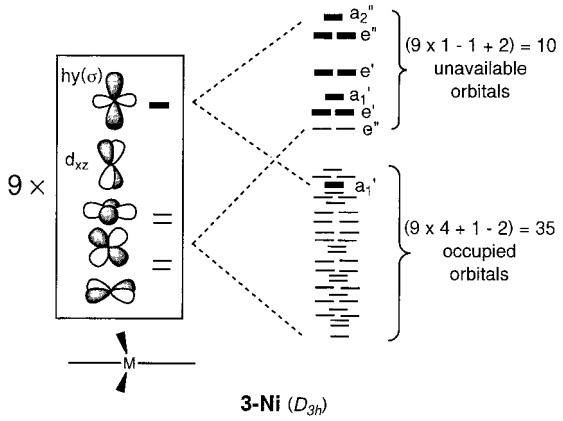

3-Ni (D_{3h})

Figure 4. Molecular orbital interaction diagram for $[Ni_9(\mu_4\text{-}S)_3(\mu_3\text{-}S)_6(PH_3)_6]^{2+}$ (**3-Ni**).

a_{1g} MO, and antibonding e_g and t_{1u} MOs that are all occupied. Thus through-space M−M bonding is canceled (see above). Similarly, complete population of the metallic d band and the antibonding set of cluster orbitals would lead to a count of 78 MEs (156 CVEs), which is the upper limit of the electron count of such a cluster. Despite the fact that the upper MOs are somewhat M−E antibonding, species with such a count should be obtained.

Condensed Octahedral $Ni_{3n}E_{3n}L_6$ Species. Interestingly enough, condensed octahedral compounds with nickel adopt a slightly different arrangement than **2**, in which the two outer metal triangular faces are not capped by chalcogenide ligands (see **3**−**5**). In other words, they do not have square-pyramidal coordinated metal centers.[17−19]

$[Ni_9(\mu_4\text{-}S)_3(\mu_3\text{-}S)_6(PEt_3)_6]^{2+}$. Approximately all metal centers in this three-stacked-triangle nickel cluster are tetracoordinated. Each ML_4 fragment resembles the one described above for the corresponding Co cluster. The metal−metal bonding in this species can be derived by considering the orbital interactions among the frontier d orbitals of the nine ML_4 fragments. Figure 4 shows the relevant orbital interaction diagram of the 70-ME (136-CVE) model cluster $[Ni_9(\mu_4\text{-}S)_3(\mu_3\text{-}S)_6(PH_3)_6]^{2+}$ (**3-Ni**) of D_{3h} symmetry obtained from EHT calculations. As in the case of cluster **2-Co**, only one bonding molecular orbital (of a'_1 symmetry) is generated from the orbital interaction of hy(σ) FOs. The other eight orbitals are antibonding and are higher in energy because of second-order mixing with the low-lying d orbitals. These d orbitals generate a set of 36 metallic MOs, two of which (of e″ symmetry) are sufficiently antibonding to be separated from the rest of the orbitals and to lie close to the antibonding set (see Figure 4). These two antibonding MOs are also derived predominantly from the high-energy d_{xz} FO, as mentioned above for **2-Co**, and have antibonding character between all neighboring metal atoms. These MOs are completely unoccupied for the count of the 70 MEs (136 CVEs) in the $[Ni_9S_9(PEt_3)_6]^{2+}$ cluster. These MEs are contained in 35 MOs (i.e., $9 \times 4 + 1\ (a'_1) - 2(e'')$). The EHT HOMO−LUMO gap is calculated to be 0.93 eV. Examination of the occupied metallic d band indicates that the M−M bonding is far from its maximum value. As noted for **2-Co**, the top of this band is M−M antibonding (except

(41) Fedorov, V.; Elsegood, M. R. J.; Yarovoi, S. S.; Mironov, Y. V. *Chem. Commun.* **1998**, 1861.
(42) Gougeon, P. Personal communication.
(43) Gautier, R.; Gougeon, P.; Halet, J.-F.; Potel, M.; Saillard, J.-Y. *J. Alloys Compd.* **1997**, *262*−*263*, 311.

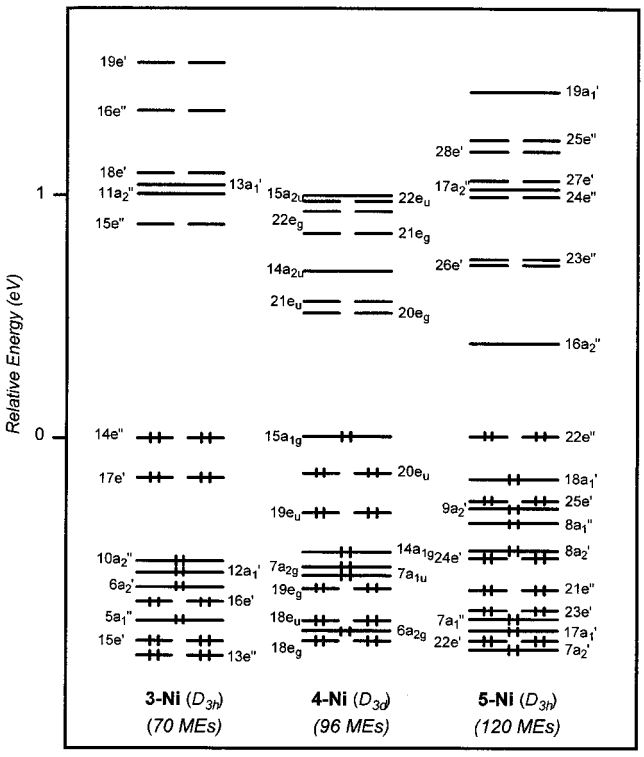

Figure 5. DFT-MO diagrams for $[Ni_9(\mu_4\text{-}S)_3(\mu_3\text{-}S)_6(PH_3)_6]^{2+}$ (**3-Ni**), $Ni_{12}(\mu_4\text{-}Se)_6(\mu_3\text{-}Se)_6(PH_3)_6$ (**4-Ni**), and $Ni_{15}(\mu_4\text{-}E)_9(\mu_3\text{-}E)_6(PH_3)_6$ (**5-Ni**).

the a'_1 MO), which leads to weak M−M bonding as illustrated by the long Ni−Ni bond distances measured experimentally in $[Ni_9S_9(PEt_3)_6]^{2+}$ (2.68−2.96 vs 2.49 Å in the elemental metal).[17] Again, this kind of arrangement is governed by M−E interactions rather than by M−M interactions.

Similar results were obtained from DFT calculations. The DFT-MO diagram of the optimized **3-Ni** structure, shown on the left-hand side of Figure 5, indicates a HOMO−LUMO gap of 0.85 eV, which confirms that $[Ni_9S_9(PEt_3)_6]^{2+}$ is diamagnetic. The bond distances obtained from the optimization of **3-Ni** under the D_{3h} symmetry constraint are collected in Table 3 and are in agreement with the corresponding experimental Ni−Ni, Ni−S, and Ni−P distances. The largest deviation concerns the Ni_o−Ni_o bond distances, which were computed to be 0.06 Å longer than the corresponding experimental bond distances.

We wonder why the ligands that cap the outer triangular faces in structural arrangement **2**, observed with cobalt, are not present in the nickel species; rather, it adopts structural arrangement **3**. EHT calculations were performed on the hypothetical 66-ME (144-CVE) $[Ni_9S_{11}(PH_3)_6]^{2+}$ model complex, the outer faces of which were capped by μ_3-S atoms. The MO diagram of this model can be constructed from the interactions of the MOs of the uncapped $[Ni_9S_9(PH_3)_6]^{2+}$ fragment (which is similar to **3-Ni**) with the six FMOs of the two capping sulfur atoms. There are three FMOs per S atom, and the fourth orbital contains a lone pair that does not participate in M−S bonding. As previously mentioned, a HOMO−LUMO gap is observed for **3-Ni** , which has 70 MEs (136 CVEs). Upon the capping of **3-Ni**, the six sulfur FMOs that contain eight electrons interact strongly with six occupied metallic MOs that are mainly localized on the outer triangles. The former set is stabilized, but the latter set is destabilized. Being partially occupied with eight electrons, this is an unfavorable situation, with electrons occupying antibonding orbitals and no HOMO−LUMO gaps. In other words, when capping occurs, metal-based MOs become unavailable because they are converted into Ni−S antibonding MOs. Consequently, structural arrangement **2**, which contains S atoms capping the outer triangular faces, is unlikely to occur with nickel because of electronic factors. However, a substantial HOMO−LUMO gap is found for a count of 58 MEs (136 CVEs), which is the favorable electron count for **2-Co**$^+$ (see above).

It is noteworthy that models $[Co_9Se_{11}(PPh_3)_6]^+$ (**2-Co**$^+$) and $[Ni_9S_9(PH_3)_6]^{2+}$ (**3-Ni**) have the same number of CVEs, namely 136, but a different number of MEs, 58 versus 70, respectively. Their electronic structures can be compared. Six occupied M−E bonding MOs lying at low energy in **2-Co**$^+$ are replaced by six occupied metallic MOs in the d band of **3-Ni**. Significant DFT HOMO−LUMO gaps are computed for both models.

$Ni_{12}(\mu_4\text{-}Se)_6(\mu_3\text{-}Se)_6(PEt_3)_6$ and $Ni_{15}(\mu_4\text{-}E)_9(\mu_3\text{-}E)_6(PPh_3)_6$ (E = S or Se). As for the Ni_9 cluster discussed above, the four-stacked-triangle $Ni_{12}Se_{12}(PEt_3)_6$[18] and the five-stacked-triangle $Ni_{15}Se_{15}(PPh_3)_6$[18] and $Ni_{15}S_{15}(PPh_3)_6$[19] clusters are composed of only tetracoordinated metal centers. Following a similar strategy, we consider their metal−metal orbital interactions on the basis of the split Ni d orbitals in an ML_4 coordination environment. Figures 6 and 7 show the relevant orbital interaction diagrams that are based on EHT calculations for the model complexes $Ni_{12}Se_{12}(PH_3)_6$ (**4-Ni**) of D_{3d} symmetry and $Ni_{15}Se_{15}(PH_3)_6$ (**5-Ni**) of D_{3h} symmetry, respectively.

In the 96-ME (180-CVE) Ni_{12} model **4-Ni**, the hy(σ) FOs give rise to a set of 12 MOs, two of which are strongly bonding (of a_{1g} and a_{2u} symmetry) and 10 of which are antibonding after second-order mixing with the metallic d orbitals. Among the 48 metallic MOs that are derived from the nonbonding or approximately nonbonding frontier fragment d orbitals of the 12 ML_4 units, two of e_g symmetry are sufficiently antibonding to be separated from the others and to be close in energy to the antibonding set, which is formed from the hy(σ) FOs. As with the corresponding orbitals in **3-Ni**, the two e_g orbitals are derived predominantly from the high-energy d_{xz} fragment orbitals. Such a situation leads to a number of 48 orbitals ($12 \times 4 - 2 + 2 = 48$) that are available to the metal d electrons of $Ni_{12}Se_{12}(PEt_3)_6$ (see Figure 6).

These results are confirmed by DFT calculations carried out on **4-Ni**. The DFT-MO diagram corresponding to the optimized geometry of **4-Ni** of D_{3d} symmetry is shown in the middle of Figure 5. A closed-shell electron configuration is computed for the count of 96 MEs (180 CVEs), with a gap of 0.54 eV. For comparison with the experimental structure of $Ni_{12}Se_{12}(PEt_3)_6$,[18] pertinent bond lengths are given for **4-Ni** in Table 3. The optimized geometry is in reasonable agreement with the experimental structure. The Ni−Se

Table 3. Comparison between the Averaged Experimental Distances of $[Ni_9S_9(PEt_3)_6]^{2+}$, $Ni_{12}Se_{12}(PEt_3)_6$, and $Ni_{15}Se_{15}(PPh_3)_6$ and the Computed Distances in the Corresponding Models $[Ni_9S_9(PH_3)_6]^{2+}$ (**3-Ni**), $Ni_{12}Se_{12}(PH_3)_6$ (**4-Ni**), and $Ni_{15}Se_{15}(PH_3)_6$ (**5-Ni**)

distance	$[Ni_9S_9(PEt_3)_6]^{2+}$, (Å)	$[Ni_9S_9(PH_3)_6]^{2+}$ (**3-Ni**), (Å)	$Ni_{12}Se_{12}(PEt_3)_6$, (Å)	$Ni_{12}Se_{12}(PH_3)_6$ (**4-Ni**), (Å)	$Ni_{12}Se_{12}(PPh_3)_6$, (Å)	$Ni_{15}Se_{15}(PH_3)_6$ (**5-Ni**), (Å)
			intratriangle			
Ni_o-Ni_o[a]	2.86	2.92	2.95	2.79	2.99	2.76
Ni_i-N_{ii}	2.96	2.97	2.91	2.87	2.90	2.84
$Ni_{ii}-N_{iii}$		2.71			2.84	2.86
			intertriangle			
Ni_o-N_{ii}	2.69	2.71	2.76	2.69	2.79	2.68
Ni_i-N_{ii}			2.77	2.66		
Ni_i-N_{iii}					2.74	2.66
			intratriangle			
Ni_o-S_o	2.15	2.17	2.27	2.26	2.28	2.26
Ni_i-S_i	2.20	2.22	2.33	2.33	2.33	2.32
$Ni_{ii}-Se_{ii}$					2.31	2.32
Ni−P	2.20	2.20	2.16	2.10	2.19	2.12

[a] See structures **3**−**5** for the labels on the atoms.

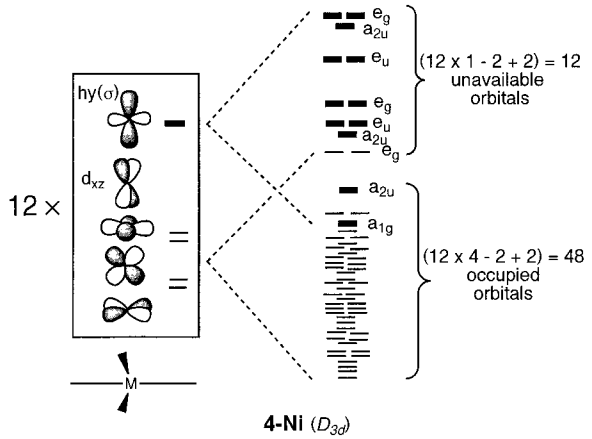

Figure 6. Molecular orbital interaction diagram for $Ni_{12}(\mu_4\text{-Se})_6(\mu_3\text{-Se})_6(PH_3)_6$ (**4-Ni**).

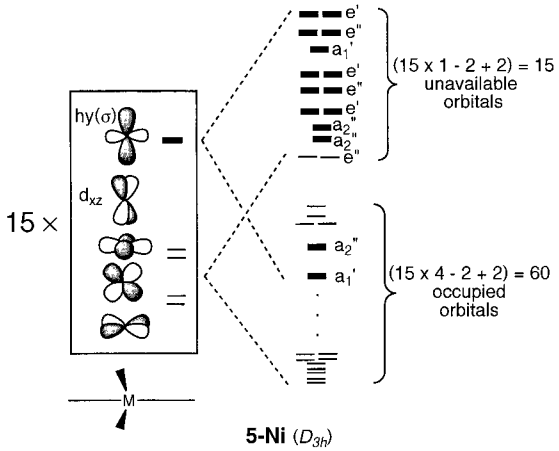

Figure 7. Molecular orbital interaction diagram for $Ni_{15}(\mu_4\text{-E})_9(\mu_3\text{-E})_6(PH_3)_6$ (**5-Ni**).

distances are reproduced with remarkably good accuracy, with a deviation of about 0.01 Å. On the other hand, the calculated Ni−Ni and Ni−P separations are about 0.05−0.15 and 0.06 Å shorter than the experimental values, respectively.

An electronic structure comparable to that of **4-Ni** is computed for the model $Ni_{15}Se_{15}(PH_3)_6$ (**5-Ni**) of D_{3h} symmetry. Again, two bonding molecular orbitals of a'_1 and a''_2 symmetry are generated from the orbital interactions of the 15 hy(σ) FOs of the ML_4 units (see Figure 7). The other 13 MOs are antibonding and lie at rather high energy. The orbital interactions among the nonbonding and approximately nonbonding metallic orbitals give a set of 60 MOs, two of which (of e″ symmetry) are antibonding between all neighboring metal atoms and are derived from the d_{xz} orbitals. These two MOs lie at rather high energy among the block of the antibonding MOs of hy(σ) parentage. Therefore, the total number of MOs that are available to metal d electrons is 60 (i.e., $15 \times 4 - 2 + 2$), which accommodate 120 MEs. Indeed, the two Ni_{15} clusters that were characterized[18,19] provide examples of the full occupation of the 60 available MOs. This qualitative approach that is based on EHT calculations is supported by DFT calculations that were carried out on **5-Ni**. The DFT-MO diagram of **5-Ni**, optimized under the D_{3h} symmetry constraint, indicates a closed-shell electron configuration with a HOMO−LUMO gap of 0.41 eV. As was observed for **4-Ni**, the bond distances computed for the five-stacked-triangle model **5-Ni** are in good agreement with the corresponding distances measured in $Ni_{15}Se_{15}(PPh_3)_6$ (see Table 3).

Longer Oligomeric Chains. According to Fenske, it is possible that larger clusters that conform to this structural arrangement exist.[3b] Chemical reactions indicate that in addition to the characterized Co and Ni compounds, residues are often obtained that, according to analytical results, seem to be of very high molecular weight. Because these residues are insoluble, it is difficult to characterize them.[3b] EHT calculations were carried out on the hypothetical models $Ni_{18}Se_{18}(PH_3)_6$, $Ni_{21}Se_{21}(PH_3)_6$, $Ni_{24}Se_{24}(PH_3)_6$, and $Ni_{27}Se_{27}(PH_3)_6$. MO diagrams (not shown here) show significant HOMO−LUMO gaps of 0.75, 0.56, 0.46, and 0.54 eV for the dicationic Ni_{18}, neutral Ni_{21}, neutral Ni_{24}, and dianionic Ni_{27} models, respectively. Analysis of the occupied and vacant metallic MOs indicates that the bonding mode in these hypothetical species is similar to that observed in smaller $Ni_{3n}E_{3n}(PR_3)_6$ species ($n = 3, 4, 5$), as described above. From these theoretical calculations, we find no reason for this kind of long oligomeric chain to be unstable.

Concluding Remarks

Although it has long been believed that the bonding picture of the late-transition-metal chalcogenide clusters composed of face-sharing octahedra was very difficult to describe, attempts to understand the electronic structures of these clusters using a simple molecular orbital approach complemented by DFT calculations have proved to be successful. In this simple molecular orbital approach, we first examined the coordination environment of each metal center and then considered the relevant d orbital splitting in such an environment on the basis of the simple ligand-field idea. We provide a convenient way to analyze complicated orbital spectra derived from molecular orbital calculations. With the aid of our analyses, we conclude that cobalt cluster **2** adopts a doublet ground state, whereas nickel clusters are all diamagnetic. It is likely that diamagnetic cobalt species $\mathbf{2}^{+}$ could be isolated.

Acknowledgment. Z.L. thanks the Research Grants Council of Hong Kong. R.G., J.-F.H. and J.-Y.S. thank the Centre de Ressources Informatiques (CRI) of Rennes and the Institut de Développement et de Ressources en Informatique Scientifique (IDRIS-CNRS) for the use of their computing facilities. We also thank Professor D. Fenske (Karlsruhe, Germany) for helpful discussions and Dr. J. Zhong (Hong Kong) for carefully reading the manuscript.

Appendix

EHT Calculations. The molecular orbital calculations were performed using the extended Hückel method.[44] The exponent (ζ) and the valence shell ionization potential (H_{ii} in eV) were, respectively,1.3, −13.6 for H 1s; 1.60, −18.6 for P 3s; 1.60, −14.0 for P 3p; 1.817, −20.0 for S 3s; 1.827, −13.3 for S 3p; 2.44, −19.5 for Se 4s; 2.07, −12.5 for Se 4p; 2.0, −9.21 for Co 4s; 2.0, −5.29 for Co 4p; 2.10, −10.95 for Ni 4s; and 2.10, −6.27 for Ni 4p. H_{ii} values for Co 3d and Ni 3d were set equal to −13.18 and −14.20, respectively. A linear combination of two Slater-type orbitals with exponents $\varsigma_1 = 5.55$ and $\varsigma_2 = 1.90$ and weighting coefficients $c_1 = 0.5551$ and $c_2 = 0.6461$ and $\varsigma_1 = 5.75$ and $\varsigma_2 = 2.00$ with weighting coefficients $c_1 = 0.5683$ and $c_2 = 0.6292$ was used to represent the Co 3d and Ni 3d atomic orbitals, respectively.

Clusters **1**−**5** were modeled by replacing all PR_3 (R = Ph or Et) ligands by PH_3. The P−H and M−P bond lengths were fixed at 1.48 and 2.19 Å, respectively, and the tetrahedral bond angle was used for PH_3. Average bond lengths from experimental data were used for both M−M and M−L bonds (except for M−P bonds). D_{3d} symmetry was used for M_{3n} clusters with even values of *n*, and D_{3h} symmetry was used for M_{3n} clusters with odd values of *n*. For cluster **1-Co**, the average Co−Co and Co−Se distances were set at 3.00 and 2.35 Å, respectively. For cluster **2-Co**, the average Co−Co and Co−Se distances within a layer were fixed at 2.92 and 2.35 Å, respectively, while those between layers were fixed at 2.79 and 2.45 Å, respectively. For clusters **3-Ni** and **5-Ni**, the average Ni−Ni and Ni−S distances within a layer were set at 2.95 and 2.18 Å, respectively, while those between layers were set at 2.69and 2.25 Å, respectively. For cluster **4-Ni**, the average Ni−Ni and Ni−Se distances within a layer were 2.93 and 2.30 Å, respectively, while those between layers were 2.77 and 2.39 Å, respectively. For the larger hypothetical models ($Ni_{18}Se_{18}(PH_3)_6$, $Ni_{21}Se_{21}(PH_3)_6$, $Ni_{24}Se_{24}(PH_3)_6$, and $Ni_{27}Se_{27}(PH_3)_6$, the average Ni−Ni and Ni−Se distances within a layer were fixed at 2.90 and 2.30 Å, repectively, while those between layers were fixed at 2.75and 2.37 Å, respectively.

DFT Calculations. Density functional calculations were carried out using the Amsterdam density functional (ADF)[45] program developped by Baerends and co-workers.[46] Electron correlation was treated within the local density approximation (LDA).[47] Becke exchange[48] and Perdew correlation[49] nonlocal (NL) gradient corrections were included in the LDA for models **1**, **2**, and **3**. These corrections were not included for larger species to reduce computational effort. The geometry optimization procedure was based on the method developed by Versluis and Ziegler.[50] An uncontracted triple-ζ Slater-type orbital (STO) basis set was used for the 3d and 4s atomic orbitals of cobalt and nickel and for the atomic orbitals of the other atoms augmented with one *n*d-STO polarization function for P, S, and Se and one 2p-STO polarization function for H. A single-ζ STO basis was used for the 4p atomic orbitals of cobalt and nickel. A frozen-core approximation[46a] was used to treat the core electrons of Ni and Co (1s−3p), P and S (1s−2p), and Se (1s−3d).

IC010812B

(44) (a) Hoffmann, R. *J. Chem. Phys.* **1963**, *39*, 1397. (b) Hoffmann, R.; Lipscomb, W. N. *J. Chem. Phys.* **1962**, *36*, 2179; Hoffmann, R.; Lipscomb, W. N. *J. Chem. Phys.* **1962**, *36*, 3189; Hoffmann, R.; Lipscomb, W. N. *J. Chem. Phys.* **1962**, *37*, 2872.

(45) *Amsterdam Density Functional (ADF) program*, release 2.3; Vrije Universiteit: Amsterdam, The Netherlands, 1997.

(46) (a) Baerends, E. J.; Ellis, D. E.; Ros, P. *Chem. Phys.* **1973**, *2*, 41. (b) Baerends, E. J.; Ros, P. *Int. J. Quantum Chem.* **1978**, *S12*, 169. (c) Boerrigter, P. M.; te Velde, G.; Baerends, E. J. *Int. J. Quantum Chem.* **1998**, *33*, 87. (d) te Velde, G.; Baerends, E. J. *J. Comput. Phys.* **1992**, *99*, 84.

(47) Vosko, S. H.; Wilk, L.; Nusair, M. *Can. J. Phys.* **1980**, *58*, 1200.

(48) Becke, A. D. *Phys. Rev. A: At., Mol., Opt. Phys.* **1988**, *38*, 3098.

(49) (a) Perdew, J. P. *Phys. Rev. B: Condens. Matter* **1986**, *33*, 8822. (b) Perdew, J. P. *Phys. Rev. B: Condens. Matter* **1986**, *34*, 7046.

(50) Versluis, L.; Ziegler, T. *J. Chem. Phys.* **1988**, *88*, 322.